The Role of Oleic Acid: From Synthesis to Assembly of Perovskite Nanocuboid Two-Dimensional Arrays

Linhua Hu,*[†,‡] Chuandao Wang,[‡] Robert M. Kennedy,[†] Laurence D. Marks,*[‡] and Kenneth R. Poeppelmeier*[†,§]

[†]Department of Chemistry, [‡]Department of Materials Science and Engineering, Northwestern University, Evanston, Illinois 60208, United States

[§]Chemical Sciences and Engineering Division, Argonne National Laboratory, Argonne, Illinois 60439, United States

S Supporting Information

ABSTRACT: Oleic acid, an 18-carbon chain fatty acid, has been widely used as a surfactant to fabricate colloidal nanocrystals. In previous work, we discovered a lamellar microemulsion strategy to fabricate sub-20 nm $SrTiO_3$ nanocuboids using oleic acid and oleate species. Here, we demonstrate (i) the general synthesis with lamellar microemulsions of a family of compositionally varied $Ba_xSr_{1-x}TiO_3$ crystalline nanocuboids with uniform size, and (ii) subsequent assembly into two-dimensional arrays by nanoparticle-bound oleate in a nonpolar solvent. The measured interparticle distance (2.4 nm) of adjacent nanoparticles in an array is less than the length of a double oleate layer (~4 nm). On the basis of calculations of the interfacial free energy, we propose the hydrophobic, hydrocarbon-terminated groups of oleate from adjacent nanocuboids are situated closely but do not overlap. Lower aspect ratio nanocuboids are bordered by four adjacent nanocuboids which results in a uniform direction self-assembly array, whereas higher aspect ratio nanocuboids are bordered by five or six adjacent nanocuboids and can develop an arced local coordination.

Self-assembly of low aspects ratio nanocuboids

Self-assembly of high aspects ratio nanocuboids
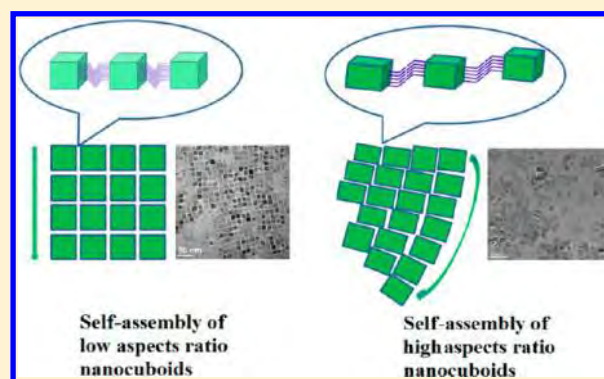
INTRODUCTION

Two-dimensional (2D) or three-dimensional (3D) nanomaterial arrays have attracted considerable attention in different fields in the last two decades, including photonics, thermoelectrics, photovoltaics, catalysis, sensors, and piezoelectric materials. Various nanomaterial synthesis methods and self-assembly processes have been reported for noble metals, semiconductors, and metal oxides.[1−4] For instance, Li et al. demonstrated an emulsion-based bottom-up self-assembly to three-dimensional colloidal spheres,[5] with further calcination into mesoporous materials,[6] and their application in high temperature catalysis.[7] Yamada et al. prepared a nanocrystal bilayer "tandem catalyst" for ethylene hydroformylation with MeOH where single layers of Pt metal nanocubes and CeO_2 metal oxide cubes were deposited sequentially.[8] Wang et al. fabricated ZnO nanowire arrays for piezoelectric nanogenerators.[9] Murray et al. investigated 2D binary nanocrystal super lattice membranes and 3D binary super lattices of magnetic nanocrystals and semiconductor quantum dots.[10−12]

The fabrication of perovskite-type nanomaterials has been discussed in numerous publications;[13−20] however, simultaneous controllable synthesis with uniform shape, size, composition, and well-defined surface is still difficult, owing to the high pH typically used in methods such as the hydrothermal process. Recently, we successfully fabricated sub-20 nm $SrTiO_3$ nanocuboids in a lamellar microemulsion

formed by oleic acid.[21] It was shown that quasi 2D nucleation and a Kinetic−Wulff growth mode (e.g., ref 22 and references therein) determined the cuboid shape for the nanocrystal growth.

Here, we continue to explore the synthesis of the family of cubic $Ba_xSr_{1-x}TiO_3$ ($0 \leq x \leq 1$) crystalline nanocuboids and their self-assembly process. As-prepared $Ba_xSr_{1-x}TiO_3$ ($0 \leq x \leq 1$) nanocuboids with surfaces covered in oleate can be well dispersed in a cyclohexane solution, and dispersed on TEM grids. As the sample dries, the nanocuboids self-assemble into arrays on the grids. The particle−particle interactions in the self-assemblies of nanocuboids on the grids is analyzed by modeling the interface energy between oleate and cyclohexane.

EXPERIMENTAL SECTION

Materials Synthesis. $Ba_xSr_{1-x}TiO_3$ ($0 \leq x \leq 1$) nanocuboids: 1.5 mmol $Ti(OBu)_4$ was added to 52.5 mL ethanol, 7.5 mL oleic acid, and 300 mg sodium oleate to form solution A, $1.5x$ mmol $Ba(Ac)_2$ and $1.5(1 − x)$ mmol $Sr(Ac)_2$ in 15 mL water was used to form solution B, 1.2 g NaOH in 6 mL water to form solution C. Solution B and C were successively added to solution A and mixed while stirring for a few minutes, with a pH of 13−14, and the resultant solution was sealed in

a 125 mL autoclave, then heated at a rate 2 °C/h to160 °C, and held for 8 h before cooling down.

Chemicals. All chemicals were of analytical grade and were used as received without further purification. Distilled water without CO_2 was used throughout, Ti(OBu)$_4$ (99%), oleic acid (90%), Sr(Ac)$_2$ (99%), Ba(Ac)$_2$ (99%), sodium oleate (99%), ethanol were supplied by Alfa Aesar Company.

Electron Microscopy. The size and morphology of the nanocrystals were determined using a Hitachi H8100 and a HD2300 scanning transmission electron microscope both at 200 kV, and a high-resolution electron microscope (HREM) and scanning transmission electron microscope JEOL 2100F at 200 kV. For high angle annular dark field (HAADF) imaging the inner and outer angle of the detector was 124 mrad and 268 mrad. Electron energy loss spectroscopy (EELS) and energy dispersive X-ray analysis (EDX) were performed to verify the composition of Ba and Sr. Samples were prepared by placing several drops of a cyclohexane dispersion of the as-prepared materials on the surface of a carbon film supported on a copper grid.

X-ray Powder Diffraction. X-ray powder diffraction of the samples was recorded using a Rigaku D/Max VB2+/PC diffractometer with Cu Ka radiation at 40 kV and 20 mA.

■ RESULTS AND DISCUSSION

Ba$_x$Sr$_{1-x}$TiO$_3$ $(0 \leq x \leq 1)$ nanocuboids can be fabricated by using different ratios of Ba and Sr precursors.

Figure 1a shows powder XRD patterns of as-prepared Ba$_x$Sr$_{1-x}$TiO$_3$ $(0 \leq x \leq 1)$ nanocuboids. BaTiO$_3$ and SrTiO$_3$ can be indexed as cubic perovskites with $Pm3m$ space group for
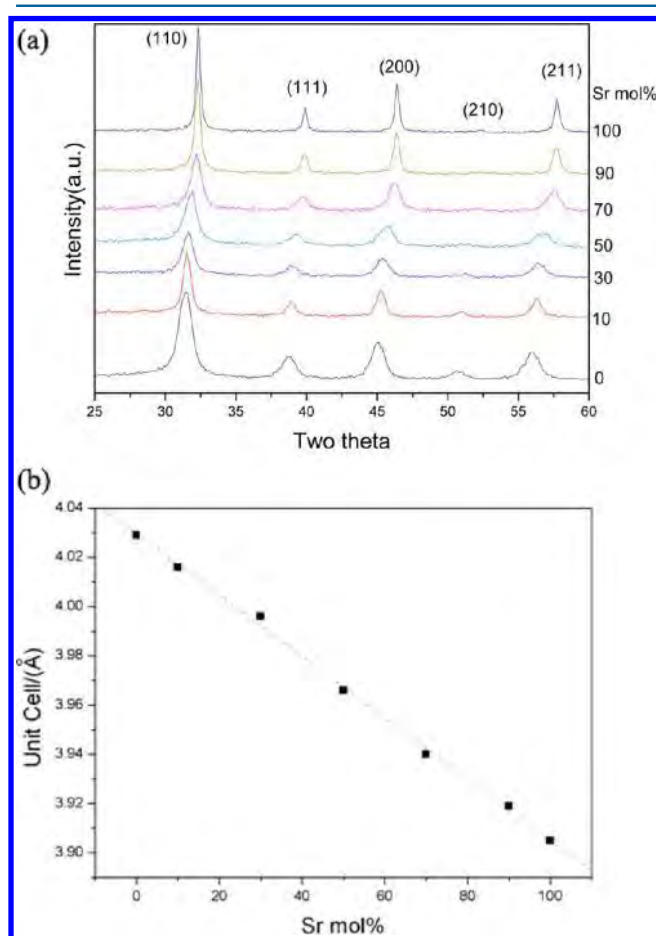

Figure 1. (a) Powder XRD patterns of Ba$_x$Sr$_{1-x}$TiO$_3$ ($x = 0, 0.1, 0.3, 0.5, 0.7, 0.9, 1$) nanocuboids. (b) Evolution of the unit cell volume with increasing Sr content.

ICDD #75-0213 and ICDD # 73-0661, respectively. While BaTiO$_3$ nanoparticles as small as 10 nm can be ferroelectric,[23] the distortion is small enough that it will be concealed by the Debye–Scherrer broadening averaged over different particle sizes in the PXRD. The unit cell of Ba$_x$Sr$_{1-x}$TiO$_3$ $(0 \leq x \leq 1)$ decreases from 4.034 Å ($x = 1$) to 3.905 Å ($x = 0$) with increasing Sr mole content. The substitution of Sr does not observably change the cubic structure.

Figure 2a shows a typical transmission electron microscope (TEM) image of 10−12 nm BaTiO$_3$ nanocuboids forming an ordered single layer on the TEM grid. Owing to their uniformity and average length/width aspect ratio of ∼1.08, each nanocuboid is bordered by four adjacent edge and four adjacent corner nanocuboids with the same orientation. Figure 2b shows a typical TEM image of BaTiO$_3$ nanocuboids where many nanocuboids are linearly arranged. Figure 3 shows a typical HREM image of an individual BaTiO$_3$ nanocuboid with {100} surfaces and well-ordered lattice fringes of 0.283 nm from the {110} planes.

Figure 4a,b shows typical TEM images of 10−15 nm Ba$_{0.5}$Sr$_{0.5}$TiO$_3$ nanocuboids. By measuring the dimensions of a representative collection of nanocuboids, an average length/width aspect ratio of 1.24 was calculated, as seen in Figure 4c. Unlike BaTiO$_3$ nanocuboids, which have a total of eight nearest neighbors, Ba$_{0.5}$Sr$_{0.5}$TiO$_3$ nanocuboids can self-assemble into arrays with five to eight nearest neighbors. This variance in the self-assembly is a result of the ratio of length and width differing from a true nanocube (length/width = 1). The TEM image in Figure 5a shows 10 Ba$_{0.5}$Sr$_{0.5}$TiO$_3$ nanocuboids that are part of an extended array, and numbered for identification. In this example, nanocuboids No. 0 and 3 are bordered by six nearest neighbors, and No. 4 has five nearest neighbors. The longest side of an average Ba$_{0.5}$Sr$_{0.5}$TiO$_3$ nanocuboid (the "length" dimension) is face−face adjacent with two different nanocuboids, instead of one for a BaTiO$_3$ nanocuboid. Such self-assembly can be hindered by larger nanocuboids. There is additional space between particles No. 10 and 2, as a result of the large size of particle No. 10 disrupting the packing. Figure 5b shows a typical HREM image of Ba$_{0.5}$Sr$_{0.5}$TiO$_3$ nanocuboid with well-ordered lattice fringes of 0.279 nm from the {110} planes. Similar to the BaTiO$_3$ nanocuboids, {100} surfaces are exposed. In our previous work, sub-20 nm SrTiO$_3$ nanocuboids with an average length/width aspect ratio of ∼1.4 were synthesized, and they formed self-assembled arrays with greater disorder than nanocuboids with lower strontium content.[21] The average length/width aspect ratio increases from 1.08, to 1.24, to 1.4 with the mole percent increase of Sr ($x = 1, 0.5, 0$). The BaTiO$_3$ nanocuboids are closest in aspect ratio to nanocubes (L/W = 1), exhibiting the least anisotropic growth.

Figure 6 shows the EELS spectrum of Ba$_{0.5}$Sr$_{0.5}$TiO$_3$ and BaTiO$_3$ nanocuboids, respectively. The peak height of the Ti L and O K edges of the Ba$_{0.5}$Sr$_{0.5}$TiO$_3$ nanocuboid are similar to those of the BaTiO$_3$ nanocuboid, while the peak height of the Ba M edge is approximately half that of the BaTiO$_3$ nanocuboid. This confirms a ∼50% Ba content in the Ba$_{0.5}$Sr$_{0.5}$TiO$_3$ nanocuboids. The EDX line-scan in Figure 7 shows that Ba and Sr are uniformly dispersed.

Self-assembly of two-dimensional ordered arrays were achieved using drops of uniform nanocuboids solution of varying concentration. Figure 8 shows a HAADF image of a low concentration of BaTiO$_3$ nanocuboids with ordered single-layer self-assembled structures. Figure 9 shows a HAADF image of a high concentration of BaTiO$_3$ nanocuboids with the yellow
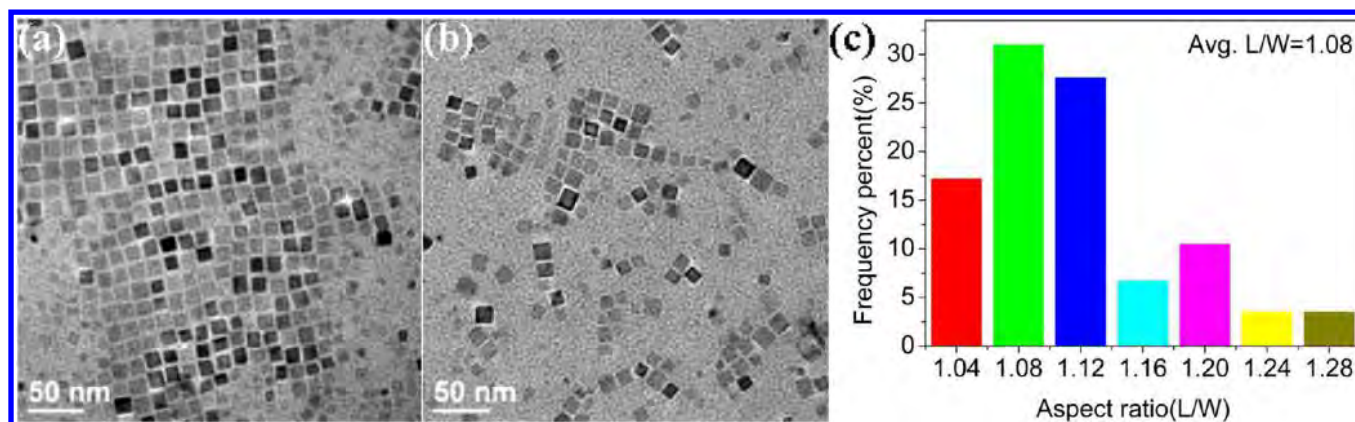
Figure 2. (a) TEM image of BaTiO$_3$ nanocuboids with single-layer self-assembly synthesized at 160 °C for 8h. (b) TEM image of BaTiO$_3$ nanocuboids with chains. (c) Aspect ratio (length/width: L/W) plot of BaTiO$_3$ nanocuboids.
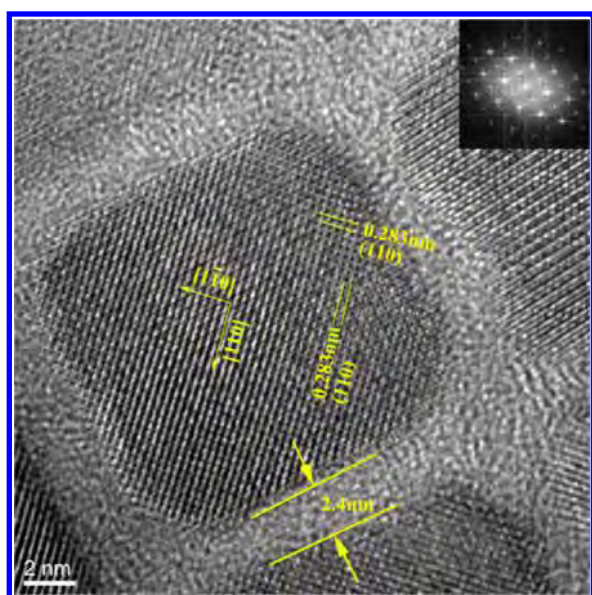

Figure 3. Typical HREM image of a BaTiO$_3$ nanocuboid.

region highlighting a single-layer, and the red region, a multilayer self-assembly packing.

Self-assembly of nanoparticles is a natural and spontaneous process occurring mainly through interactions such as van der Waals, hydrogen bonding, hydrophilic/hydrophobic, electrostatic, and metal−ligand coordination networks.[24−27] Modification of the surface of metal nanocubes with different surfactants can lead to edge−edge (PVP) or face−face (PEG) self-assembly.[28] Noncovalent interactions of long-chain molecules can lead to close-packed regular superstructures such as with hexagonal yttrium phosphate nanocrystals.[29] Although noncovalent interactions of long chain molecules associated with hydrophobic interactions and a siphonic effect have been discussed, the role of nonpolar solvent has not been closely considered for such nanoparticle self-assembly.

As shown in Figure 3, the distance of adjacent nanocuboids is ∼2.4 nm, which is larger than one layer of oleate (∼2 nm) and less than two layers of oleate (∼4 nm). To understand the self-assembly, a calculation of interface free energy between the nonpolar hexane solvent and oleate is given in the Supporting Information (SI). The capillary energy of two adjacent nanocuboids immersed in cyclohexane is 13.4×10^{-19} J, much larger than $1\ kT$ (4.04×10^{-21} J) which is the minimal resistant energy for self-assembly from infinite separation to a finite separation.[30,31] This indicates that there is a strong interaction between the oleate chains driving self-assembly.

All of the Ba$_x$Sr$_{1−x}$TiO$_3$ nanocuboids should have a similar degree of oleate coating; therefore, the driving force of self-assembly should be similar, including the interface free energy between oleate on the surface and the nonpolar solvent, and
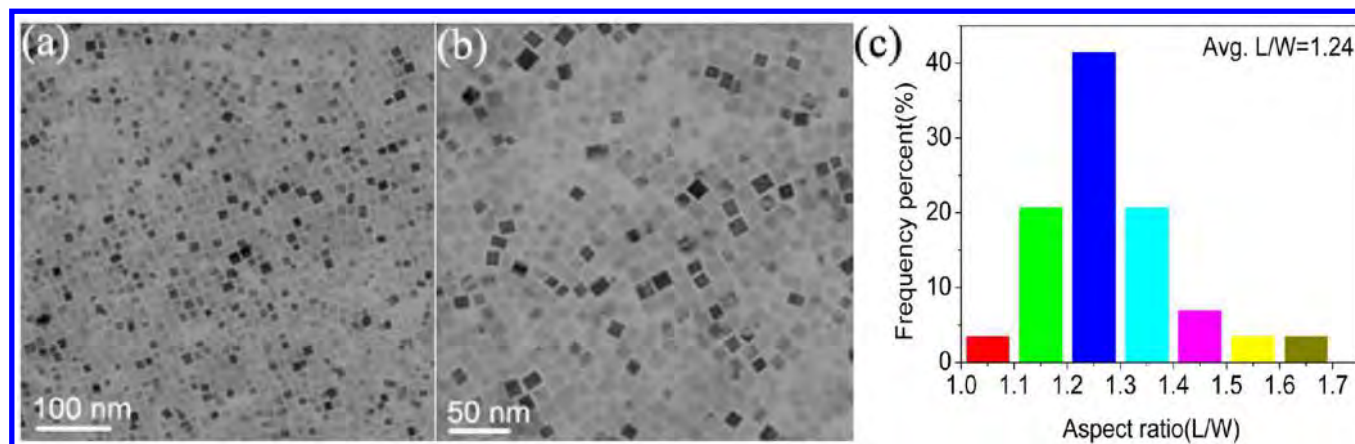

Figure 4. (a, b) TEM images of Ba$_{0.5}$Sr$_{0.5}$TiO$_3$ nanocuboids synthesized at 160 °C for 8 h. (c) Aspect ratio (length/width: L/W) plot of Ba$_{0.5}$Sr$_{0.5}$TiO$_3$ nanocuboids.
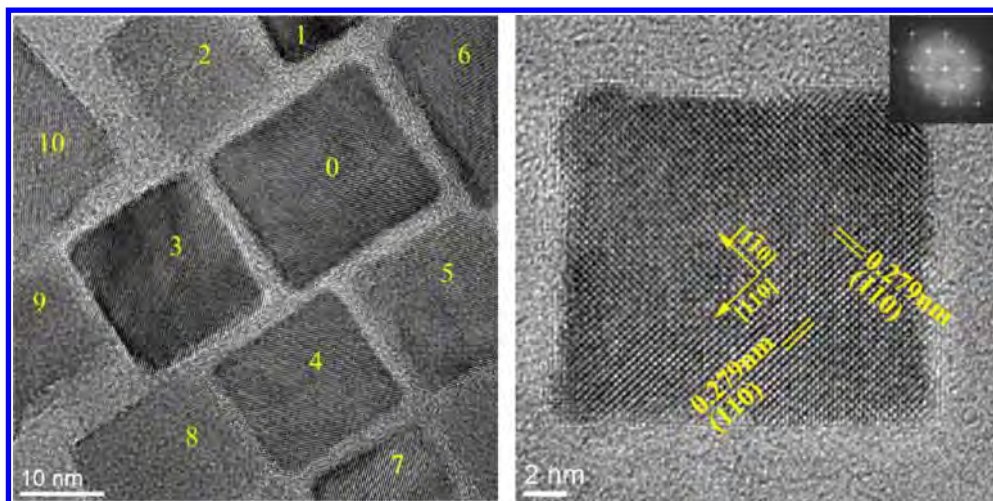
Figure 5. (a) Self-assembly of TEM image of $Ba_{0.5}Sr_{0.5}TiO_3$ nanocuboids labeled No. 0-10. (b) A typical HREM image of a $Ba_{0.5}Sr_{0.5}TiO_3$ nanocuboid.
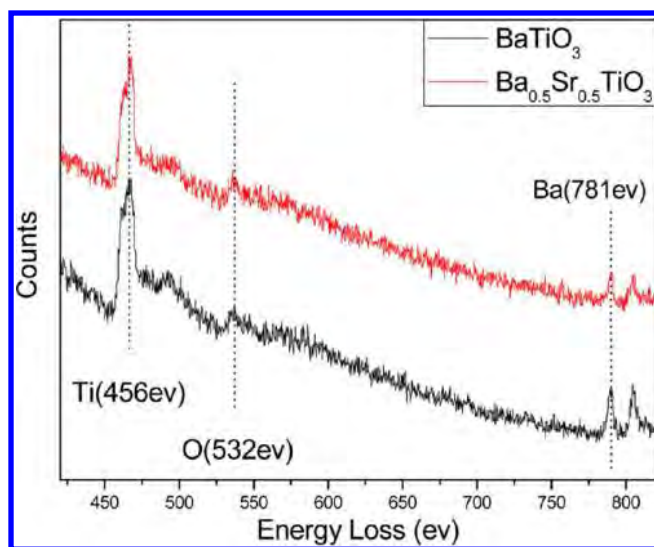

Figure 6. EELS spectrum of single $Ba_{0.5}Sr_{0.5}TiO_3$ and $BaTiO_3$ nanocuboids showing the Ti L, O K, and Ba M edges.

the van der Waals force between the oleate chains, even for nanocuboids of different aspect ratios. However, for the $Ba_xSr_{1-x}TiO_3$ series, even though the driving force for self-assembly should be similar, the nanocuboids show very different assembly patterns as the aspect ratio varies. $BaTiO_3$ nanocuboids show a uniform self-assembly into a cubic array with 90° angles, whereas as the aspect ratio increases, as with $Ba_{0.5}Sr_{0.5}TiO_3$, the nanocuboids show a multidirection self-assembly, with curved arcs of nanoparticles. We argue this is dependent on their aspect ratio (length/width). When the assembly is happening between nanocuboids with an aspect ratio sufficiently removed from unity, the long edge of a nanocuboid might be bordered by either the similar long edge of an adjacent nanocuboid or two short edges from adjacent nanocuboids. These two options and the rotation that occurs to minimize the unused space in the array lead to increasingly random assembly as the aspect ratio moves away from unity. To further illustrate the self-assembly behavior of higher aspect ratio, a TEM image of ~20 nm $SrTiO_3$ nanocuboids, Figure 10, with ~1.4 aspect ratio, is shown. These nanocuboids do not
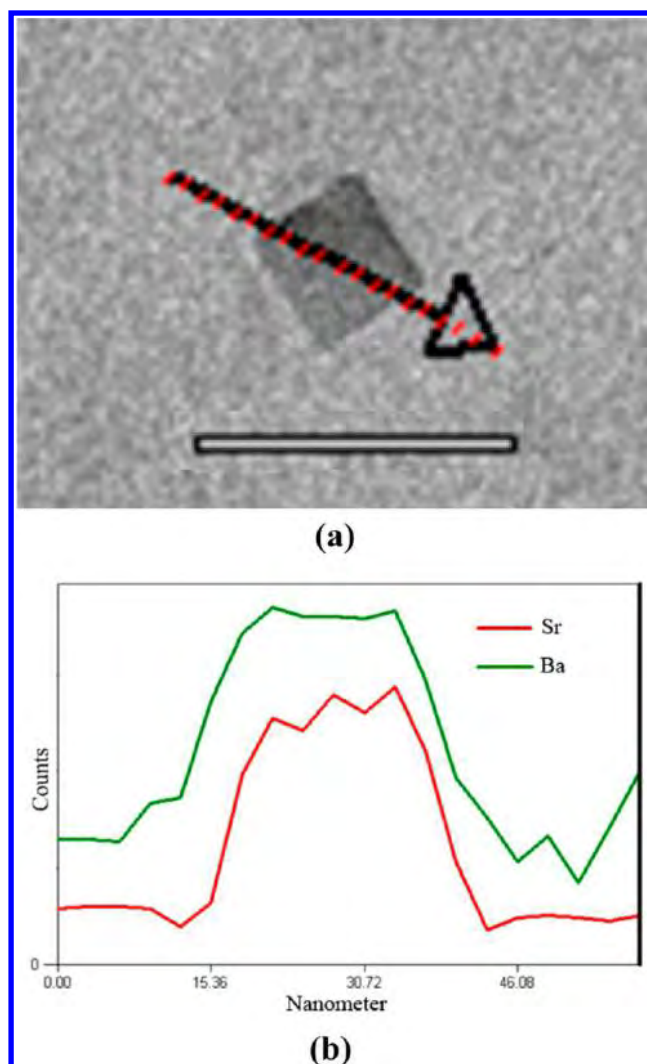

Figure 7. (a) Bright field image of a single $Ba_{0.5}Sr_{0.5}TiO_3$ nanocuboid; the red line is the EDX line scanning path; the scale bar is 50 nm. (b) EDX based compositional line profile across the particle by indicating an even distribution of Ba (upper line) and Sr (lower line) in the nanocuboid.
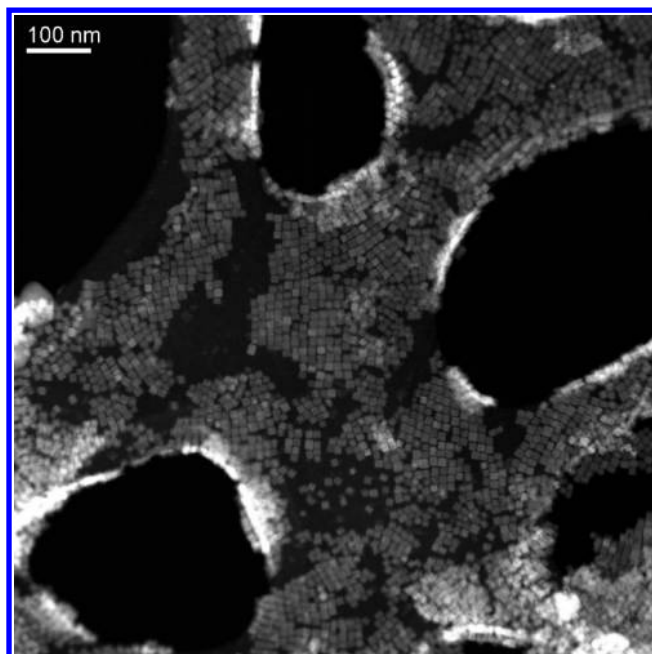
Figure 8. BaTiO$_3$ nanocuboids with single-layer self-assembly.

Figure 10. SrTiO$_3$ nanocuboids with single-layer self-assembly.
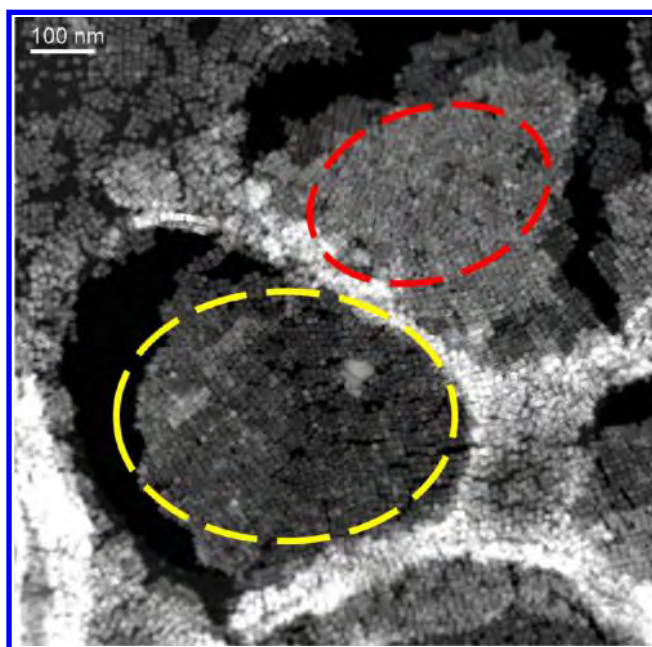

Figure 9. BaTiO$_3$ nanocuboids with single-layer (yellow) and multilayer (red) self-assembly.

form a uniform cubic 90° self-assembly but instead exhibit an obvious arc-direction self-assembly in the left corner.

CONCLUSIONS

In summary, a family of cubic Ba$_x$Sr$_{1−x}$TiO$_3$ (0 ≤ x ≤ 1) crystalline nanocuboids was successfully synthesized with simultaneous control of uniform shape, size, composition, and well-defined surface. These nanocuboids exhibit a large area of ordered two-dimensional self-assembly. The self-assembly depends upon the aspect ratio of the nanocuboids. Lower aspect ratio nanocuboids are readily self-assembled into uniform arrays, matching the high symmetry of the nanoparticles, and larger aspect ratio nanocuboids tend to show less
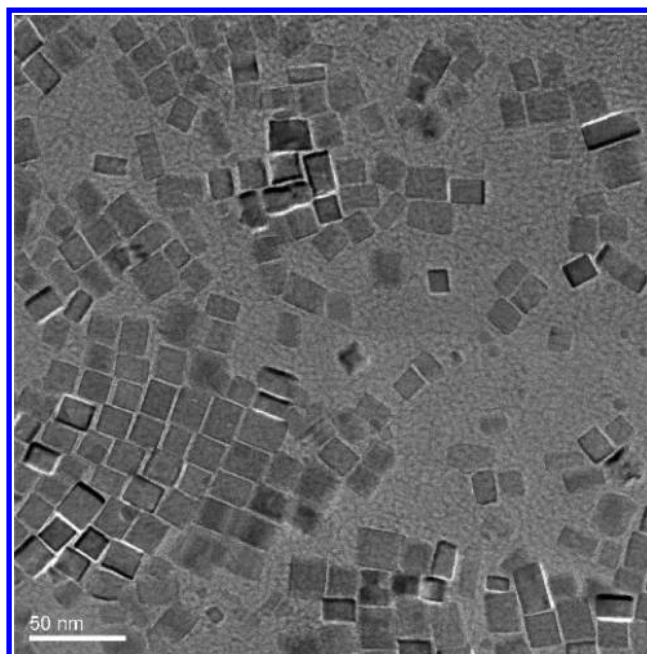
ordered self-assembly. The interactions between nanoparticles in a self-assembled array can be understood by the analysis of interface free energy of adjacent nanocuboids in a nonpolar solvent. It is believed that hydrophobic carbon chains are playing a crucial role in perovskite nanocuboids self-assembly which is different from the role played during the lamellar microemulsion synthesis.[21]

ASSOCIATED CONTENT

Ⓢ Supporting Information

Interface free energy calculation. This material is available free of charge via the Internet at http://pubs.acs.org.

AUTHOR INFORMATION

Corresponding Authors

* (L.H.) E-mail: l-hu@northwestern.edu.
* (L.D.M.) E-mail: l-marks@northwestern.edu.
* (K.R.P.) E-mail: krp@northwestern.edu.

Notes

The authors declare no competing financial interest.

REFERENCES

(1) Vanmaekelbergh, D. *Nano Today* **2011**, *6*, 419−437.

(2) Grzelczak, M.; Vermant, J.; Furst, E.; Liz-Marzán, L. *ACS Nano* **2010**, *4*, 3591−3605.

(3) Henzie, J.; Grünwald, M.; Widmer-Cooper, A.; Geissler, P. L.; Yang, P. *Nat. Mater.* **2012**, *11*, 131−137.

(4) Fendler, J. H. *Chem. Mater.* **1996**, *8*, 1616−1624.

(5) Bai, F.; Wang, D.; Huo, Z.; Chen, W.; Liu, L.; Liang, X.; Chen, C.; Wang, X.; Peng, Q.; Li, Y. *Angew. Chem., Int. Ed.* **2007**, *46*, 6650−6653.

(6) Wang, D.; Xie, T.; Peng, Q.; Li, Y. *J. Am. Chem. Soc.* **2008**, *130*, 4016−4022.

(7) Chen, C.; Nan, C.; Wang, D.; Su, Q.; Duan, H.; Liu, X.; Zhang, L.; Chu, D.; Song, W.; Peng, Q.; Li, Y. *Angew. Chem., Int. Ed.* **2011**, *50*, 3725−3729.

(8) Yamada, Y.; Tsung, C.-K.; Huang, W.; Huo, Z.; Habas, S. E.; Soejima, T.; Aliaga, C. E.; Somorjai, G. A.; Yang, P. *Nat. Chem.* **2011**, *3*, 372−376.

(9) Wang, Z. L.; Song, J. *Science* **2006**, *312*, 242−246.

(10) Redl, F. X.; Cho, K.-S.; Murray, C. B.; O'Brien, S. *Nature* **2003**, *423*, 968−971.

(11) Dong, A.; Chen, J.; Vora, P. M.; Kikkawa, J. M.; Murray, C. B. *Nature* **2010**, *466*, 474−477.

(12) Dong, A.; Ye, X.; Chen, J.; Murray, C. *Nano Lett.* **2011**, *11*, 1804−1809.

(13) Demirörs, A. F.; Imhof, A. *Chem. Mater.* **2009**, *21*, 3002−3007.

(14) Li, Y.; Gao, X. P.; Li, G. R.; Pan, G. L.; Yan, T. Y.; Zhu, H. Y. *J. Phys. Chem. C* **2009**, *113*, 4386−4394.

(15) Su, K.; Nuraje, N.; Yang, N.-L. *Langmuir* **2007**, *23*, 11369−11372.

(16) Niederberger, M.; Pinna, N.; Polleux, J.; Antonietti, M. *Angew. Chem., Int. Ed.* **2004**, *43*, 2270−2273.

(17) Rabuffetti, F. A.; Kim, H.-S.; Enterkin, J. A.; Wang, Y.; Lanier, C. H.; Marks, L. D.; Poeppelmeier, K. R.; Stair, P. C. *Chem. Mater.* **2008**, *20*, 5628−5635.

(18) Fujinami, K.; Katagiri, K.; Kamiya, J.; Hamanaka, T.; Koumoto, K. *Nanoscale* **2010**, *2*, 2080−2083.

(19) Adireddy, S.; Lin, C.; Cao, B.; Zhou, W.; Caruntu, G. *Chem. Mater.* **2010**, *22*, 1946−1948.

(20) Rabuffetti, F. A.; Brutchey, R. L. *J. Am. Chem. Soc.* **2012**, *134*, 9475−9487.

(21) Hu, L.; Wang, C.; Lee, S.; Winans, R. E.; Marks, L. D.; Poeppelmeier, K. R. *Chem. Mater.* **2013**, *25*, 378−384.

(22) Ringe, E.; Duyne, R. Van; Marks, L. *J. Phys. Chem. C* **2013**, *117*, 15859−15870.

(23) Mark J. Polking, M. N.; Myung-Geun Han, M.-G.; Yourdkhani, A.; Petkov, V.; Kisielowskim, C. R.; Volkov, V. V.; Zhu, Y.; Caruntu, G.; Alvisatos, A. P.; Ramesh, R. *Nat. Mater.* **2012**, *11*, 700−709.

(24) Whitesides, G. M.; Grzybowski, B. *Science* **2002**, *295*, 2418−2421.

(25) Murray, C.; Kagan, C.; Bawendi, M. *Science* **1995**, *270*, 1335−1338.

(26) Maye, M. M.; Lim, I.-I. S.; Luo, J.; Rab, Z.; Rabinovich, D.; Liu, T.; Zhong, C.-J. *J. Am. Chem. Soc.* **2005**, *127*, 1519−1529.

(27) Collier, C. P.; Vossmeyer, T.; Heath, J. R. *Annu. Rev. Phys. Chem.* **1998**, *49*, 371−404.

(28) Gao, B.; Arya, G.; Tao, A. R. *Nat. Nanotechnol.* **2012**, *7*, 433−437.

(29) Huo, Z.; Chen, C.; Li, Y. *Chem. Commun.* **2006**, *1*, 3522−3524.

(30) Davis, H. T. *Statistical Mechanics of Phases, Interfaces and Thin Films*; Wiley-VCH: New York, 1996.

(31) Bowden, N.; Terfort, A.; Carbeck, J.; Whitesides, G. M. *Science* **1997**, *276*, 233−235.